Rev. Adv. Mater. Sci. 48 (2017) 142-146

MECHANICAL PROPERTIES OF GRAPHENE CONTAINING ELONGATED TETRAVACANCIES (575757-666-5757 DEFECTS)

A.S. Kochnev[1,2], I.A. Ovid'ko[1,2,3] , B.N. Semenov[1,2,3] and Ya.A. Sevastyanov[1,2]

[1]Peter the Great St. Petersburg Polytechnic University, St. Petersburg 195251, Russia
[2]St. Petersburg State University, St. Petersburg 199034, Russia
[3]Institute of Problems of Mechanical Engineering, Russian Academy of Sciences, St. Petersburg 199178, Russia

Received: December 4, 2016

Abstract. Classical molecular dynamics (MD) with the adaptive intermolecular reactive bond order (AIREBO) potential is used to examine the effects of elongated tetravacancies (575757-666-5757 defects) on the mechanical properties of graphene sheets containing such defects. In these computer simulations, stress-strain dependences, maximum elastic strain, maximum plastic strain and tensile strength are revealed which characterize a graphene sheet containing an elongated tetravacancy in two tensile tests. In the first and second tests, tensile load was applied parallel and perpendicular to the long axis of the defect, respectively. It is revealed that the mechanical characteristics of graphene are significantly influenced by elongated tetravacancies.

1. INTRODUCTION

Graphene exhibits the excellent mechanical properties which are important for a wide range of applications; see, e.g., [1-3]. For instance, following the experimental data [1], pristine graphene is characterized by extraordinarily high strength of around 130 GPa. Real graphene sheets, membranes and layers (on substrates) typically contain structural defects strongly affecting their mechanical and functional properties; see, e.g., reviews [4-6]. So, following experimental data, computer simulations and theoretical examinations, tensile strength of graphene degrades due to the presence of grain boundaries, line defects carrying orientation mismatch between adjacent graphene crystallites (grains) [2,5,7-16]. Also, point defects like Stone-Wales defects, disclinations, vacancies, divacancies and point-like tetravacancies (5559 defects) in graphene can decrease its strength; see molecular dynamics simulations [17-25]. At the same time, along with grain boundaries, Stone-Wales defects, disclinations, vacancies, divacancies and point-like tetravacancies (5559 defects), 575757-666-5757 defects – elongated tetravacancies - can be present in graphene sheets due to irradiation [26]. In particular, elongated 575757-666-5757 tetravacancies are among the four most frequently observed tetravacancy defects in monolayer graphene under electron irradiation [26]. Generally speaking, such tetravacancies are capable of strongly affecting both strength and thus lifetime of graphene specimens under mechanical load. In this context, there is large interest in description of deformation and fracture processes in graphene containing exended tetra-

Corresponding author: I.A. Ovid'ko, e-mail: ovidko@def.ipme.ru

vacancies and examination of its mechanical properties. The main aims of this paper are to perform computer simulations addressing the effects of elongated tetravacancies on the mechanical characteristics (stress-strain dependences, maximum elastic strain, maximum plastic strain and tensile strength) of graphene sheets containing such defects.

Each 575757-666-5757 defect represents an elongated tetravacancy consisting of five pairs of "pentagon-heptagon" configurations that surround three "hexagon" configurations of carbon atoms (Fig. 1). Thus, geometry of an elongated tetavacancy is "intermediate" between geometries of line and point defects. With this factor, there is interest in analysis of the influence of tensile load direction on the deformation behavior exhibited graphene containing a containing an elongated tetravacancy. In the context discussed, in our research, we will perform two tensile tests with tensile load being applied parallel and perpendicular to the long axis of the elongated tetravacancy.

2. SIMULATION METHOD

In description of deformation and fracture processes in graphene sheets containing elongated tetravacancies, we used the Large-scale Atomic/Molecular Massively Parallel Simulator MD simulation package. In order to specify interatomic bonds, the adaptive intermolecular reactive bond order (AIREBO) potential [27] was utilized. The initial simulation cell has a square-like shape with sizes 10 nm x 10 nm and is characterized by periodic boundary conditions along directions parallel to its edges. The distance between carbon atoms in graphene in its initial state is taken as 1.42 Å. More details on the simulation method can be found in Ref. [20].

At the first stage of the pre-simulation procedure, we created an elongated 575757-6666-5757 tetravacancy whose long axis is parallel to a zigzag axis (Fig. 1). At the second stage of the pre-simulation procedure, the defected graphene model was relaxed through simulations involving 1,000,000 iteration steps in Nose-Hoover thermostat at room temperature (300K).

Then the tensile strain was applied with a strain rate of 0.001 ps^{-1}. In the first tensile test, the tension was applied along the armchair direction perpendicular to the long axis of the elongated tetravacancy. In the second tensile test, the tension was applied along the zigzag direction parallel to the long axis of the elongated tetravacancy. Evolution of the graphene sheets in the tensile tests will be considered in detail in next section.

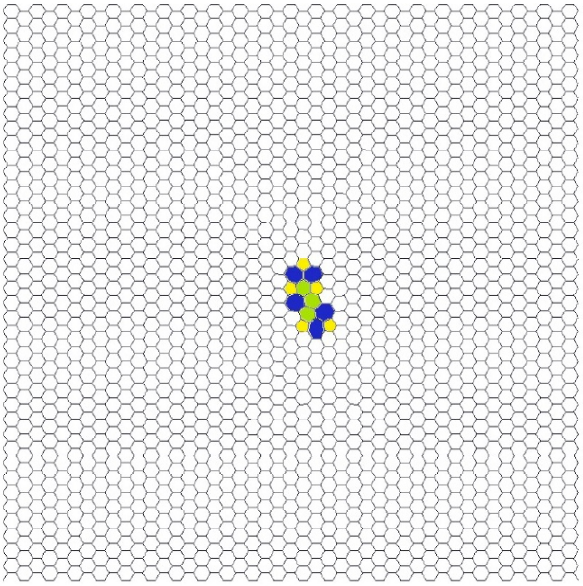

Fig. 1. Graphene sheet containing an elongated 575757-666-5757 tetravacancy. 5- and 7-disclinations composing the tetravacancy are shown as yellow pentagons and blue heptagons, respectively. Hexagons belonging to the tetravacancy are colored green.

3. DEFORMATION AND FRACTURE PROCESSES IN GRAPHENE SHEET WITH ELONGATED TETRAVACANCY

Following our simulations, evolution of a graphene sheet containing the elongated tetravacancy under tension in the zigzag direction (parallel to the tetravacancy long axis) is illustrated in Fig. 2. When the tensile load is applied to the graphene sheet, structural defects carrying plastic deformation and fracture are generated in the sheet, first of all, in the vicinity of the pre-existent tetravacancy (Fig. 2a). Basic defects that carry plastic flow are pairs of 5- and 7-disclinations and seldom other configurations (Fig. 2a). Defects that carry fracture are crack/void-like *n*-cells, that is, *n*-membered rings of carbon atoms, where $n > 7$ (for details, see a discussion in Ref. [25]). Fig. 2a shows a graphene sheet containing a large void nucleus resulted from convergence of several crack/void-like *n*-cells.

Further elongation of the graphene sheet under tension load is accompanied by generation of new n-disclinations and their convergence with pre-existent disclinations (Fig. 2b). These processes result in the formation of a large void bounded by highly deformed graphene areas containing high densities

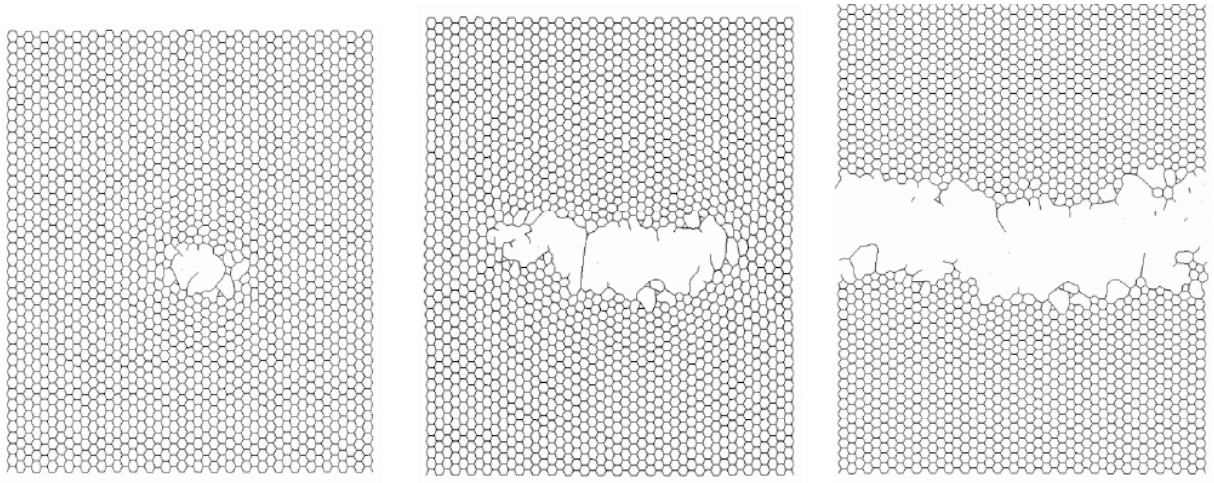

Fig. 2. Evolution of graphene containing an elongated tetravacancy under tensile load along the zigzag direction of graphene hexagonal lattice. Structure of graphene sheet is shown at (a) $\varepsilon \approx 27\%$; (b) $\varepsilon \approx 30.3\ \%$; and (c) $\varepsilon \approx 40\ \%$ (for a detailed description, see the main text).

of *n*-disclinations, where *n* = 3, 4, 5, 7, 8, …. Finally, the large void catastrophically grows so that the graphene sheet in the simulation cell breaks into two separate parts (Fig. 2c).

Similar deformation and fracture processes occur in a graphene sheet containing a elongated tetravacancy under tension in the armchair direction perpendicular to the tetravacancy long axis. The main difference between the graphene sheets loaded along the armchair and zigzag directions is reflected in the corresponding stress-strain curves (Fig. 3) and their mechanical characteristics.

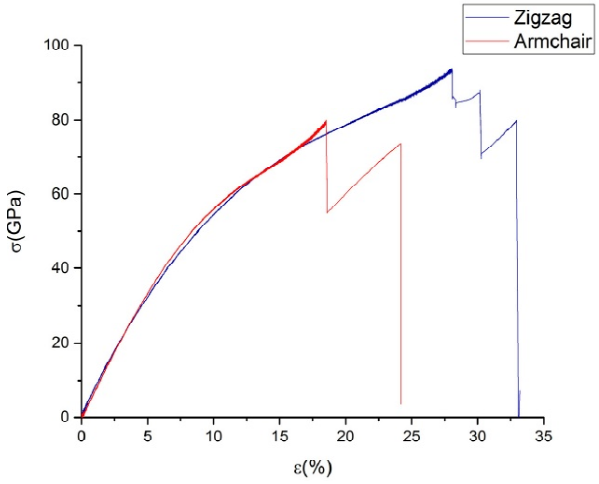

Fig. 3. Strain-stress dependences that characterize deformation and fracture processes in pristine graphene deformed along armchair and zigzag crystallographic directions (red and blue curves, respectively).

Fig. 3 presents strain-stress dependences characterizing deformation and fracture processes in graphene sheets that contain elongated tetravacancies and are deformed along the armchair and zigzag crystallographic directions, respectively. Each of the "strain-stress" dependences has the elastic and plastic deformation parts. Plastic deformation parts contain many bursts each is associated with either re-arrangement or break of an interatomic bond.

We now consider mechanical characteristics (derived from strain-stress dependences in Fig. 3) of a graphene sheet containing an elongated tetravancy, depending on the tension direction. In the situation where tension load is applied along the zigzag crystallographic direction, the maximum elastic strain $\varepsilon_{el} \approx 27\%$, the maximum plastic strain $\varepsilon_{pl} \approx 6\%$, and the tensile strength $\sigma_t \approx 94$ GPa. In the situation where tension load is applied along the armchair crystallographic direction, the maximum elastic strain $\varepsilon_{el} \approx 17\%$, the maximum plastic strain $\varepsilon_{pl} \approx 7\%$, and the tensile strength $\sigma_t \approx 80$ GPa. Values of the maximum elastic strain $\varepsilon_{el} \approx 17\%$ and » 27% are lower and near, respectively, the experimentally measured [1] value $\varepsilon_{el} \approx 25\%$ that characterizes micron-sized pristine graphene membrane. Values of the tensile strength $\sigma_t \approx 80$ GPa and ≈ 94 GPa are lower than their counterparts ($\sigma_{pr\text{-}armchair}$ = 100 GPa and $\sigma_{pr\text{-}zigzag}$ = 131 GPa, respectively; see computer simulations [20]) that specify pristine graphene.

Graphene sheets containing elongated tetravacancies are characterized by non-zero plastic strains $\varepsilon_{pl} \approx 6$ and 7% in tension tests along the zigzag and armchair crystallographic direction, respectively. It is contrasted to the brittle behavior exhibited by pristine graphene membrane [1]. Thus, graphene shows plasticity due to the presence of elongated tetravacancies. Note that other point defects also can enhance plasticity of graphene [22-24] or even initiate its superplastic behavior [25].

4. CONCLUDING REMARKS

In this paper, we performed MD simulations (with the AIREBO potential) of deformation and fracture processes occurring in graphene sheets containing elongated tetravacancies (575757-666-5757 defects). Each 575757-666-5757 defect represents an elongated tetravacancy consisting of five pairs of "pentagon-heptagon" configurations that surround three "hexagon" configurations of carbon atoms (Fig. 1). Thus, geometry of an elongated tetavacancy is "intermediate" between geometries of line and point defects. Such elongated tetravacancies are among the four most frequently observed tetravacancy defects in monolayer graphene under electron irradiation [26].

The MD simulations have shown that elastic and plastic deformation stages occur in graphene sheets containing elongated tetravacancies. After the elastic deformation stage, plastic deformation and local fracture processes (in the vicinity of the tetravacancy) occur in graphene (Figs. 2a and 2b). Basic defects that carry plastic flow are pairs of 5- and 7-disclinations and seldom other configurations. Defects that carry fracture are crack/void-like *n*-cells, that is, *n*-membered rings of carbon atoms, where $n > 7$. During the plastic deformation stage, a large void is nucleated through convergence of several crack/void-like *n*-cells (Fig. 2a). Then, the large void grows through its convergence with new crack/void-like *n*-cells intensively generated in its vicinity (Fig. 2b). Finally, the large void catastrophically grows so that the graphene sheet breaks into two separate parts (Fig. 2c).

In our simulations, we found the basic mechanical characteristics of the sheets containing elongated tetravacancies. In the situation where tension load is applied along the zigzag crystallographic direction, the maximum elastic strain $\varepsilon_{el} \approx 27\%$, the maximum plastic strain $\varepsilon_{pl} \approx 6\%$, and the tensile strength $\sigma_t \approx 94$ GPa. In the situation where tension load is applied along the armchair crystallographic direction, the maximum elastic strain $\varepsilon_{el} \approx 17\%$, the maximum plastic strain $\varepsilon_{pl} \approx 7\%$, and the tensile strength $\sigma_t \approx 80$ GPa.

With these values and their comparison with those that specify pristine graphene, we conclude that the presence of elongated tetravacancies weakly influences the maximum elastic strain and decreases (by $\approx$ 20-30%) the tensile strength. At the same time, in contrast to brittle pristine graphene [1], graphene sheets under our examination show substantial plasticity (characterized by plastic strain $\varepsilon_{pl} \approx$ 6-7%) due to the presence of elongated tetravacancies.

ACKNOWLEDGEMENTS

This work was supported, in part (for A.S.K and I.A.O.), by the Ministry of Education and Science of Russian Federation (Zadanie 9.1964.2014/K) and, in part (for B.N.S. and Y.A.S.), by St. Petersburg State University (research grant 6.38.337.2015). The simulations were performed at Resource Center "Simulation Center of St. Petersburg State University".

REFERENCES

[1] C. Lee, X. Wei, J.W. Kysar and J. Hone // *Science* **321** (2008) 385.
[2] I.A. Ovid'ko // *Rev. Adv. Mater. Sci.* **34** (2013) 1.
[3] C. Daniels, A. Horning, A. Phillips, D.V.P. Massote, L. Liang, Z. Bullard, B.G. Sumpter and V. Meunier // *J. Phys.: Condens. Matter* **27** (2015) 373002.
[4] F. Banhart, J. Kotakoski and A.V. Krasheninnikov // *ACS Nano* **5** (2011) 26.
[5] I.A. Ovid'ko // *Rev. Adv. Mater. Sci.* **30** (2012) 201.
[6] L.P. Biro and P. Lambin // *New J. Phys*. **15** (2013) 035024.
[7] P. Y. Huang, C.S. Ruiz-Vargas, A. M. van der Zande, W.S. Whitney, M.P. Levendorf, J.W. Kevek, S. Garg, J.S. Alden, C.J. Hustedt, Y. Zhu, J. Park, P.L. McEuen and D.A. Muller // *Nature* **469** (2011) 389.
[8] C.S. Ruiz-Vargas, H.L. Zhuang, P.Y. Huang, A.M. van der Zande, S. Garg, P.L. McEuen, D.A. Miller, R.C. Hennig and J. Park // *Nano Lett*. **11** (2011) 2259.
[9] R. Grantab, V.B. Shenoy and R.S. Ruoff // *Science* **330** (2010) 946.
[10] Y. Wei, J. Wu, H. Yin, X. Shi, R. Yang and M. Dresselhaus // *Nature Mater*. **11** (2012) 759.

[11] T.-H. Liu, C.-W. Pao and C.-C. Chang // *Carbon* **50** (2012) 3465.
[12] Y.I. Jhon, S.-E. Zhu, J.-H. Ahn and M.S. Jhon // *Carbon* **50** (2012) 3708.
[13] J. Zhang, J. Zhao and J. Lu // *ACS Nano* **6** (2012) 2704.
[14] I.A. Ovid'ko and A.G. Sheinerman // *J. Phys. D: Appl. Phys.* **46** (2013) 345305.
[15] A. Cao and J. Qu // *Appl. Phys. Lett*. **107** (2013) 071902.
[16] Y. Li, D. Datta and Z. Li // *Carbon* **90** (2015) 234.
[17] M.C. Wang, C. Yan, L. Ma, N. Hu and M.W. Chen // *Comput. Mater. Sci*. **54** (2012) 236.
[18] J.A. Baimova, L. Bo, S.V. Dmitriev, K. Zhou and A.A. Nazarov // *Europhys. Lett.* **103** (2013) 46001.
[19] C. Carpenter, D. Maroudas and A. Ramasubramaniam // *App. Phys. Lett.* **103** (2013) 013102.
[20] A.S. Kochnev, I.A. Ovid'ko and B.N. Semenov // *Rev. Adv. Mater. Sci.* **37** (2014) 105.
[21] A.S. Kochnev and I.A. Ovid'ko // *Rev. Adv. Mater. Sci.* **43** (2015) 89.
[22] A.S. Kochnev and I.A. Ovid'ko // *Mater. Phys. Mech.* **27** (2016) 60.
[23] A.S. Kochnev, N.F. Morozov, I.A. Ovid'ko and B.N. Semenov // *Doklady Physics.* **61** (2016) 239.
[24] A.S. Kochnev, N.F. Morozov, I.A. Ovid'ko and B.N. Semenov // *Doklady Physics.* **61** (2016) 403.
[25] A.S. Kochnev, I.A. Ovid'ko and B.N. Semenov // *Rev. Adv. Mater. Sci.* **47** (2016) 79.
[26] A.W. Robertson, G.-D. Lee, K. He, E. Yoon, A.I. Kirkland and J.H. Warner // *Nano Letters* **14** (2014) 1634.
[27] S.J. Stuart, A.B. Tutein and J.A. Harrison // *J. Chem. Phys.* **112** (2000) 6472.